Acta Mech Sin (2007) 23:485–493
DOI 10.1007/s10409-007-0102-5

RESEARCH PAPER

A new bionic MAV's flapping motion based on fruit fly hovering at low Reynolds number

Peng Bai · Erjie Cui · Feng Li · Weijiang Zhou · Bingyan Chen

Received: 19 July 2006 / Revised: 29 April 2007 / Accepted: 9 May 2007 / Published online: 4 September 2007

Abstract On the basis of the studies on the high unsteady aerodynamic mechanisms of the fruit fly hovering the aerodynamic advantages and disadvantages of the fruit fly flapping motion were analyzed. A new bionic flapping motion was proposed to weaken the disadvantages and maintain the advantages, it may be used in the designing and manufacturing of the micro air vehicles (MAV's). The translation of the new bionic flapping motion is the same as that of fruit fly flapping motion. However, the rotation of the new bionic flapping motion is different. It is not a pitching-up rotation as the fruit fly flapping motion, but a pitching-down rotation at the beginning and the end of a stroke. The numerical method of 3rd-order Roe scheme developed by Rogers was used to study these questions. The correctness of the numerical method and the computational program was justified by comparing the present CFD results of the fruit fly flapping motion in three modes, i.e., the advanced mode, the symmetrical mode and the delayed mode, with Dickinson's experimental results. They agreed with each other very well. Subsequently, the aerodynamic characteristics of the new bionic flapping motion in three modes were also numerically simulated, and were compared with those of the fruit fly flapping. The conclusions could be drawn that the high unsteady lift mechanism of the fruit fly hovering is also effectively utilized by this new bionic flapping. Compared with the fruit fly flapping, the unsteady drag of the new flapping decreases very much and the ratio of lift to drag increases greatly. And the great discrepancies among the mean lifts of three flapping modes of the fruit fly hovering are effectively smoothed in the new flapping. On the other hand, this new bionic flapping motion should be realized more easily. Finally, it must be pointed out that the above conclusions were just drawn for the hovering flapping motion. And the aerodynamic characteristics of the new bionic flapping motion in forward flight are going to be studied in the next step.

Keywords Flapping wing · Low Reynolds number · MAV's · Unsteady · Numerical simulation

The project supported by the National Natural Science Foundation of China (10232010, 10032060, 90605005).

P. Bai (✉) · E. Cui · F. Li · W. Zhou · B. Chen
China Academy of Aerospace Aerodynamics,
Beijing 100074, China
e-mail: baipeng73@yahoo.com.cn

1 Introduction

The aerodynamics of the flapping wings at low Reynolds number has become one of the research focuses because of the rapid development of the micro air vehicles (MAV's) technologies recently. The earliest literatures about the flapping wings were the observation notes of Leonardo da Vinci in 1500 [1]. The first person who studied the details of the flapping wing flight was Etienne–Jules Marey in the middle of the nineteenth century [1]. He took photos of the bird flight in 11 frames per second, with the camera designed by himself. And the research paper about the flapping wings appeared in NACA reports [2] and J. Exp. Biol periodical [3] in the first half of the twentieth century. But the systematic and effective studies about the flapping wing flight were not carried out until recent twenty years. Especially, lots of deep researches about the flapping wing of the fruit fly (*Drosophila*) were published [4–13], and many significant progresses were made.

The purpose of studying the insect flapping flight is to understand how and why animals can obtain their special abilities and to make use of them to benefit the human kinds. It is important and significant to study and design a new bionic flight structure with simpler flapping movements than the insects. The structure can generate higher unsteady aerodynamic lift, lower drag and energy dissipation, and higher ratio of lift to drag than the fruit fly can.

A new kind of bionic flapping manner was proposed in this paper on the basis of the systematical analyses about the unsteady aerodynamic mechanisms of the fruit fly hovering. The numerical scheme developed by Rogers [14] was used to simulate the unsteady flowfields of three modes of the fruit fly flapping and this new bionic flapping. The flapping parameters used in the simulations were obtained from the observations and the experiments of Weis-Fogh, Vogel and Dickinson etc. The correctness and effectiveness of these simulations were proven through comparing the present CFD results of fruit fly flapping and Dickinson's experimental results [5]. Then the aerodynamic mechanisms and the aerodynamic discrepancies between this new bionic flapping and the fruit fly flapping were studied in detail.

2 Numerical method

The governing equations and the numerical method used in this paper is the same as Sun and Tang's paper [7],which was developed by Roger's [14]. The governing equations of the flow are the dimensionless unsteady incompressible Navier–Stokes equations in the inertial frame *XYZ* (see Fig. 1):

$$\begin{aligned}
&\frac{\partial u}{\partial X}+\frac{\partial v}{\partial Y}+\frac{\partial w}{\partial Z}=0,\\
&\frac{\partial u}{\partial t}+u\frac{\partial u}{\partial X}+v\frac{\partial u}{\partial Y}+w\frac{\partial u}{\partial Z}\\
&\quad=-\frac{\partial p}{\partial X}+\frac{1}{Re}\left(\frac{\partial^2 u}{\partial^2 X}+\frac{\partial^2 u}{\partial^2 Y}+\frac{\partial^2 u}{\partial Z^2}\right),\\
&\frac{\partial v}{\partial t}+u\frac{\partial v}{\partial X}+v\frac{\partial v}{\partial Y}+w\frac{\partial v}{\partial Z}\\
&\quad=-\frac{\partial p}{\partial Y}+\frac{1}{Re}\left(\frac{\partial^2 v}{\partial^2 X}+\frac{\partial^2 v}{\partial^2 Y}+\frac{\partial^2 v}{\partial Z^2}\right),\\
&\frac{\partial w}{\partial t}+u\frac{\partial w}{\partial X}+v\frac{\partial w}{\partial Y}+w\frac{\partial w}{\partial Z}\\
&\quad=-\frac{\partial p}{\partial Z}+\frac{1}{Re}\left(\frac{\partial^2 w}{\partial^2 X}+\frac{\partial^2 w}{\partial^2 Y}+\frac{\partial^2 w}{\partial Z^2}\right).
\end{aligned} \tag{1}$$

The equations that transformed from the Cartesian coordinates system (X, Y, Z, t) to the curvilinear coordinates system (ξ, η, ζ, τ) are written in conservative form as follows: Continuity equation:

$$\frac{\partial}{\partial \xi}\left(\frac{U}{J}\right)+\frac{\partial}{\partial \eta}\left(\frac{V}{J}\right)+\frac{\partial}{\partial \varsigma}\left(\frac{W}{J}\right)=0, \tag{2a}$$

Momentum equation:

$$\frac{\partial \hat{u}}{\partial t}=-\frac{\partial}{\partial \xi}\left(\hat{e}-\hat{e}_v\right)-\frac{\partial}{\partial \eta}\left(\hat{f}-\hat{f}_v\right)-\frac{\partial}{\partial \zeta}\left(\hat{g}-\hat{g}_v\right)=-\hat{r}, \tag{2b}$$

where J is the Jacobian of the transformation. $\hat{r}$ is the right hand side.

$$\begin{aligned}
&\xi=\xi(X,Y,Z,t), \quad \eta=\eta(X,Y,Z,t),\\
&\varsigma=\varsigma(X,Y,Z,t), \quad \tau=t.
\end{aligned} \tag{3}$$

The numerical method is based on the method of artificial compressibility, which introduces a pseudo-time derivative of pressure into the continuity equation. The time accuracy of this numerical algorithm is achieved by subiterating in pseudo-time for each physical time step. The convective terms are split through Roe's third-order flux-difference technique. The viscous terms are split by a second-order central difference. And the time derivatives in the momentum equation are differenced by a second-order, three-points, backward-difference formula. In order to accelerate the speed of convergence, the LGS implicit method was used during the subiteration. Then the governing equations are transferred to the following form:

$$\left[I_{tr}+\left(\frac{\partial \hat{R}}{\partial \hat{D}}\right)^{n+1,m}\right]\left(\hat{D}^{n+1,m+1}-\hat{D}^{n+1,m}\right)$$

$$=-\hat{R}^{n+1,m}-\frac{I_m}{\Delta t}\left(1.5\hat{D}^{n+1,m}-2\hat{D}^{n}+0.5\hat{D}^{n-1}\right), \tag{4}$$

$$\begin{aligned}
&I_{tr}=\mathrm{diag}\left[\frac{1}{\Delta\tau},\frac{1}{\Delta\tau}+\frac{1.5}{\Delta t},\frac{1}{\Delta\tau}+\frac{1.5}{\Delta t},\frac{1}{\Delta\tau}+\frac{1.5}{\Delta t}\right],\\
&I_m=\mathrm{diag}[0,1,1,1],
\end{aligned} \tag{5}$$

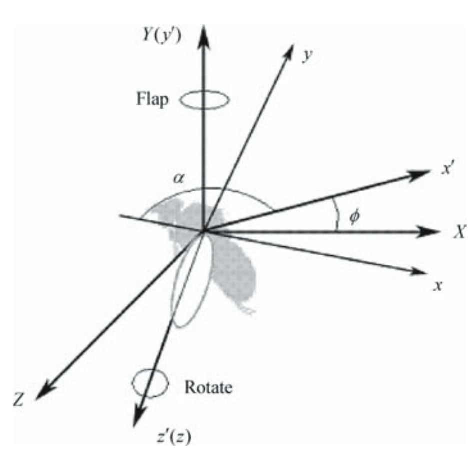

Fig. 1 Illustration of the movement of the flapping wing

$$\hat{D} = \frac{1}{J}\begin{bmatrix} p \\ u \\ v \\ w \end{bmatrix}, \quad \hat{E} = \begin{bmatrix} \beta \dfrac{U}{J} \\ \hat{e} \end{bmatrix},$$
$$\hat{F} = \begin{bmatrix} \beta \dfrac{V}{J} \\ \hat{f} \end{bmatrix}, \quad \hat{G} = \begin{bmatrix} \beta \dfrac{W}{J} \\ \hat{g} \end{bmatrix}, \tag{6}$$
$$\frac{\hat{D}^{m+1} - \hat{D}^{m}}{\Delta\tau} = -\hat{R}^{m+1}.$$

The details of this numerical method are listed in Ref. [14].

Because of the translation and rotation of the flapping wing without morphing in this study, the body-conforming grid in the body-fixed non-inertial frame (xyz. see Fig. 1) is generated only once, which does not need to alter with time. The computational grid in the inertial frame (*XYZ*. see Fig. 1) is obtained by the time-dependent coordinate transformation and relationship between the inertial and non-inertial frames of reference. And the governing equations are solved in the inertial frame of reference. This approach has some advantages. The far-field boundary conditions do not need to be treated specially, and the existing numerical methods can be directly used. The wall boundary conditions are written in following:

$$\boldsymbol{U} = \boldsymbol{U}_B, \quad \frac{\partial p}{\partial n} = -\rho \boldsymbol{a}_B \cdot \boldsymbol{n},$$

where $\boldsymbol{U}_B$ and $\boldsymbol{a}_B$ are the velocity and acceleration of the wall, and $\boldsymbol{n}$ is the normal vector of the wall.

3 The computational grids

The model wing of the fruit fly (*Drosophila*) used in the present computational simulation to verify the numerical methods is the same as Dickinson's experiments [5]. And the new model wing used to study the new bionic flapping is obtained through averaging the shapes of the leading edge and the trailing edge of Dickinson's model without changing the area and the distribution of the chord. The body-fixed grid in the non-inertial frame is the O-H type (see Fig. 2). The planform and grid of the fruit fly flapping model wing are shown in Fig. 2a, and those of the new flapping model wing is shown in Fig. 2b.

The airfoils of both model wings are flat with two half-circle ends, the mean chord c is 8.79cm with 0.05c thickness, and the ratio of length to chord λ is 2.84. The airfoil is shown in Fig. 2c. The computational grids have dimensions of 81×65×70 around the wing section in the normal direction and in the spanwise direction. The outer boundary is set at 15 chord lengths from the wing. The normal grid spacing at the wall is 0.002 chord length.

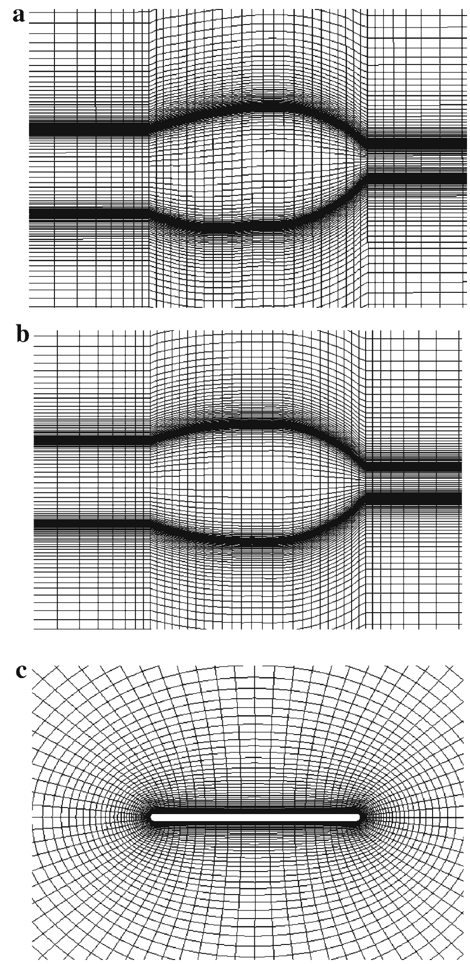

Fig. 2 The computational grid of flapping wing. **a** Computational grid for the fruit fly wing; **b** computational grid for the study of the new flapping manner; **c** the airfoil of the flapping wing

4 Introduction of the flapping motion

The motion of the flapping wing is shown in Fig. 1. There are three frames in the Fig. 1. Following the biomechanics convention, the flapping motion is divided into two parts, "upstroke" and "downstroke". The azimuthal rotation of the wing around the Y axis is called the "translation" and the pitching up or pitching down of the wing near the end of strokes is called "rotation". The (XYZ) is the inertial frame, which is fixed on the body of the insect. The (xyz) is the non-inertial frame, which is fixed on the wing of the insect. And the $(x'y'z')$ is the transforming reference frame between (XYZ) and (xyz), which translate with the flapping wing without rotation. Then the Y axis and y' axis are identical, and the z axis and z' axis are identical.

The translational angle and the rotational angle are denoted by ϕ and α, respectively. The speed at the span location r_0 is named the translational speed of the wing and denoted by u_t. And r_0 is the radius of the second moment of the wing area and is defined by $r_0 = \sqrt{\int_S r^2 \mathrm{d}S/S}$, where r is the radial distance and S is the wing area. The angular velocity of the azimuth angle is given by: $\phi_t = u_t/r_0$. The present flapping plane of the hovering is simplified to be horizontal as Dickson [5] and Sun [7]. The translational speed u_t takes a constant value U_t except at the beginning and end of a stroke, which is given by:

$$\begin{aligned} &u_t^+ = U_t^+ \sin(\pi(\tau - \tau_1)/\Delta\tau_t),\\ &\quad \tau_1 \le \tau \le \tau_1 + \Delta\tau_t/2,\\ &u_t^+ = U_t^+,\\ &\quad \tau_1 + \Delta\tau_t/2 \le \tau \le \tau_2,\\ &u_t^+ = U_t^+ \sin(\pi(\tau - \tau_2 + \Delta\tau_t/2)/\Delta\tau_t),\\ &\quad \tau_2 \le \tau \le \tau_2 + \Delta\tau_t/2, \end{aligned} \tag{7}$$

where $U_t^+ = U_t/U$, $u_t^+ = u_t/U$, U is the reference velocity taken by averaging the translational velocity u_t during one flapping period. τ is the dimensionless time, $\tau = tU/c$, where t is dimensional time, τ_1 is the beginning of the translation in a stroke, $\Delta\tau_t/2$ is the time of the acceleration at the beginning of the stroke. The time of the deceleration at the end of stroke is the same and τ_2 is the beginning of the deceleration during a stroke. Dimensionless ϕ_t^+ is determined by u_t^+.

The attack angle of the flapping wing in the middle of a stroke is fixed at 40°. The dimensionless angular velocity of the rotation at the end of stroke is given by:

$$\begin{aligned} &\alpha_t^+ = 0.5\alpha_{t0}^+[1 - \cos(2\pi(\tau - \tau_r)/\Delta\tau_r)],\\ &\quad \tau_r \le \tau \le \tau_r + \Delta\tau_r, \end{aligned} \tag{8}$$

where $\alpha_t^+ = \alpha_t c/U$, α_{t0}^+ is the constant, τ_r is the beginning of the rotation, $\Delta\tau_r$ is the time of rotation at the end of stroke. At present, the amplitude of the rotation between strokes is 100° for the fruit fly flapping. When the $\Delta\tau_r$ is given, α_{t0}^+ can be taken. The fruit fly flapping motion can be described simply that the wing translates at the constant angle of attack in the middle of a stroke, and the wing rotates to change the angle of attack through pitching up at the beginning and the end of stroke. According to the phase of the rotation respect to stroke, the motion can be devided into three modes: the advanced mode, which means that wing rotation precedes stroke reversal by 8% of the wingbeat cycle, the symmetrical mode, which means that wing rotation occurs symmetrically with respect to stroke, and the delayed mode, which means that wing rotation is delayed with respect to stroke reversal by 8% of the stroke cycle. The details of the fruit fly flapping motion can be found in Refs. [5,7].

The dimensionless parameters are calculated according to the bundling fruit fly flight experiments of Weis-Fogh [15] and Vogel [16]. The air density $\rho = 1.226\,\mathrm{kg/m^3}$, the weight of the insect is 1.96×10^{-5}N, the mass of the wing is 2.4×10^{-6} g, the length of the wing is 0.3cm, the inertial radius is 0.58, the mean chord is 0.108cm, the angular amplitude of the translation Φ is 2.62rad (=150°), the frequency of the flapping $f = 240$/s. Then the reference velocity U, the Reynolds number, the dimensionless flapping cycle τ_c, and the lift coefficient needed to resist the weight, C_{Lw} can be calculated as following: $U = 2\Phi n r_2 = 218.7\,\mathrm{cm/s}$, $Re = cU/\nu = 147$, $\tau_c = (1/n)/(c/U) \approx 8.42$, $C_{Lw} = 1.15$.

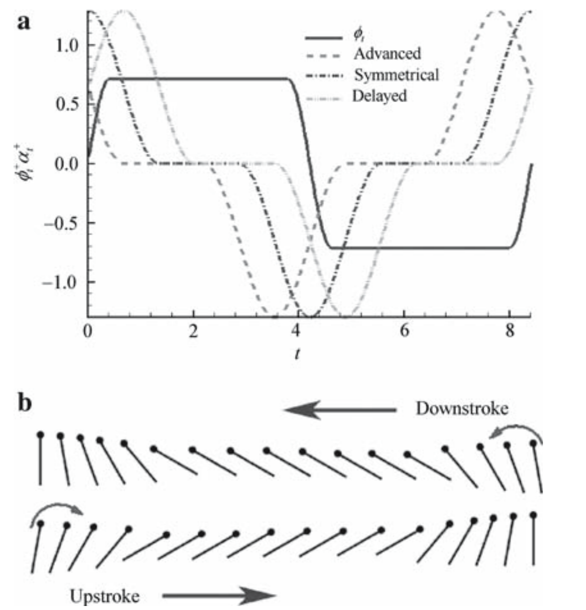

Fig. 3 The distribution of the flapping angle ϕ, the rotational angle α, and their angle velocity ϕ_t^+, α_t^+ of three modes in fruit fly flapping motion. **a** Flapping velocity and rotational velocity; **b** sketch of flapping in the symmetrical mode

In Dickinson's experiment, the oil density is $0.88\times 10^3\,\mathrm{kg/m^3}$, the wing length is 0.25 m, the wing area $S = 0.0167\,\mathrm{m^2}$, the mean chord $c = 8.79\,\mathrm{cm}$, the inertial radius is $r_2 = 0.58R$, the flapping frequency $f = 0.145\,\mathrm{Hz}$, the azimuth amplitude $\Phi = 160°$, the reference velocity $U = 2\Phi n r_2 = 0.117\,\mathrm{m/s}$, and $0.5\rho U^2 S \approx 0.101\,\mathrm{kg\,m/s^2}$.

According to the upper references, the present computational parameters are $\tau_c = 8.42$, $\Delta\tau_t = 0.1\tau_c$, $\Delta\tau_r = 0.32\tau_c$, $\Phi = 160°$, the constant angle of attack for the upstroke and downstroke α_{up} and α_{down} are 40°, the angular amplitude of the rotation $\Delta\alpha = 100°$. The azimuth Φ, rotational angle α, dimensionless translational angular velocity ϕ_t^+ and rotational angular velocity α_t^+ during one cycle can be determined (see Fig. 3).

Through analyses, the remarkable characteristics of the fruit fly flapping motion are listed as following: (1) The order of the leading edge and the trailing edge of the flapping wing does not change. The leading edge will not alter to be the trailing edge. (2) The windward and the leeward wing surfaces alternate, which means the windward surface during one stroke will become the leeward surface during the subsequent stroke. (3) The rotation used to change the angle of

Table 1 The average lift and drag coefficient and the ratio of lift to drag

Flapping mode	Advanced	Symmetrical	Delayed
Fruit fly flapping $C_{L(\text{average})}$	1.959566	1.787183	0.77392
New bionics flapping $C_{L(\text{average})}$	1.551128	1.881962	1.12484
Fruit fly flapping $C_{D(\text{average})}$	2.997	2.745	2.923
New bionics flapping $C_{D(\text{average})}$	1.757	1.740	1.697
Fruit fly flapping C_L/C_D	0.6538	0.6511	0.2648
New bionics flapping C_L/C_D	0.8828	1.0816	0.6628

$\Delta\tau_t = 0.1\tau_c$, $\Delta\tau_r = 0.32\tau_c$

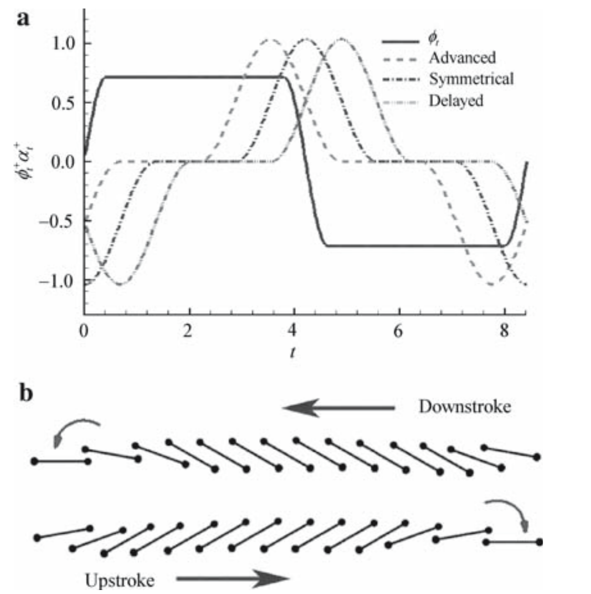

Fig. 4 The distribution of the flapping angle ϕ, the rotational angle α, and their angle velocity ϕ_t^+, α_t^+ of three modes in new flapping motion. **a** Flapping velocity and rotational velocity; **b** sketch of flapping in the symmetrical mode

attack of the flapping wing at the beginning and the end of a stroke is pitching up rapidly.

For the fruit fly flapping, there are four unsteady mechanisms, the delayed stall, the fast pitching-up rotation, the rapid acceleration and the rapid deceleration, to generate high unsteady lift. In the delayed stall mechanism, the dynamic-stall vortex is carried by the wing in its translation, which is the most important reason for the lift. In the fast pitching-up rotation mechanism, two lift peaks are generated at the beginning and the end of a stroke, but at the same time, two drag peaks are also generated, approximately two times of the lift peaks (see Fig. 6). In the rapid acceleration and deceleration mechanisms, high lift peaks are also generated at the two ends of a stroke, but these two mechanisms must work with fit angle of attack. So with the pitching-up rotation, the acceleration and deceleration mechanisms make benefits for the lift in the advanced mode and the symmetrical mode, but make loss in the delayed mode.

The conclusion can be drawn that although the pitching-up rotation mechanism with rapid acceleration and deceleration contributes lift, it also generates high drag. Then the mean unsteady drag is much bigger than the mean unsteady lift in all three modes. In the advanced mode, the mean drag is 1.53 times of the mean lift. In the symmetrical mode, it is 1.54 times. And in the delayed mode, it is 3.78 times (see Table 1). So from the view of the energy consumption, the fruit fly flapping motion is not a very highly effective flapping motion to generate high unsteady lift. So that it is very significant for designing and manufacturing MAV's to invent and study a new flapping motion, which can not only reasonably use the fruit fly mechanisms to generate high unsteady lift, but also decrease the disadvantage of the fruit fly flapping.

A new kind of bionic flapping motion based on the above analyses was proposed here. The translation of the new flapping motion is the same as the fruit fly. But the pitching-up rotation of the fruit fly flapping motion at the beginning and end of a stroke is replaced by pitching-down rotation to alter the angle of attack. Compared with the fruit fly flapping motion, the new bionic flapping motion has the following obvious characteristics: (1) The leading edge and the trailing edge of the flapping wing in the new flapping motion change alternately, which means that the leading (trailing) edge of the flapping wing in a stroke will become the trailing (leading) edge in the subsequent stroke; (2) The windward surface and the leeward surface of the flapping wing do not change in the new flapping motion; (3) For the new flapping motion, the method used to change the angle of attack is pitching down rapidly. The sketches of the symmetrical modes in the fruit fly flapping motion and the new bionic flapping motion are shown in Figs. 3 and 4. In Fig. 3, the end with solid circle means the leading edge of the flapping wing and the other end is the trailing edge. That shows that the leading edge will always be the leading edge. In Fig. 4, both ends are marked with the solid circle, which means that both sides will be the leading edge, and the leading edge and the trailing edge alternate each other.

In order to compare the aerodynamic characteristics of the new flapping motion with that of the fruit fly, except the direction of the rotation, the flapping parameters used to study the new flapping are same as that of the fruit fly. So, in this paper, α_{up} and α_{down} are 40° too, $\tau_c = 8.42$, $\Delta\tau_t = 0.1\tau_c$, $\Delta\tau_r = 0.32\tau_c$, $\Phi = 160°$, $Re = 147$, and the definition of the advanced mode, symmetrical mode and delayed mode are same. But the angular amplitude of the rotation $\Delta\alpha = 80°$. The translational speed u_t is same as that in formula (7). And although the rotation direction in the new flapping motion is different from the fruit fly, the dimensionless angular velocity of the rotation at the ends of strokes is also given by formula (8). Based on the frame references and the definition of the angle α in Fig. 2, for the fruit fly flapping motion, $\alpha_{\text{up}} = 40°$, $\alpha_{\text{down}} = 140°$, and for the new bionic flapping motion, $\alpha_{\text{up}} = 220°$, $\alpha_{\text{down}} = 140°$. Then ϕ_t^+ and α_t^+ in the fruit fly flapping motion and in the new flapping motion can all be taken (see Figs. 3 and 4).

5 Results

5.1 Verification of the calculation method

The correctness of the calculation method was proved by comparing the present CFD results of the fruit fly flapping with Dickinson's experiments [5]. The three modes, advanced mode, symmetrical mode and delayed mode, were all calculated, see Fig. 5. The computational dimensionless parameters of these modes have been given in Sect. 4. The rotational axis is located at the 25% chord length position from the leading edge, which is the same as Dickinson's experiments [5]. The computational grid is shown in Fig. 2a. The translational and rotational motions are shown in Fig. 3.

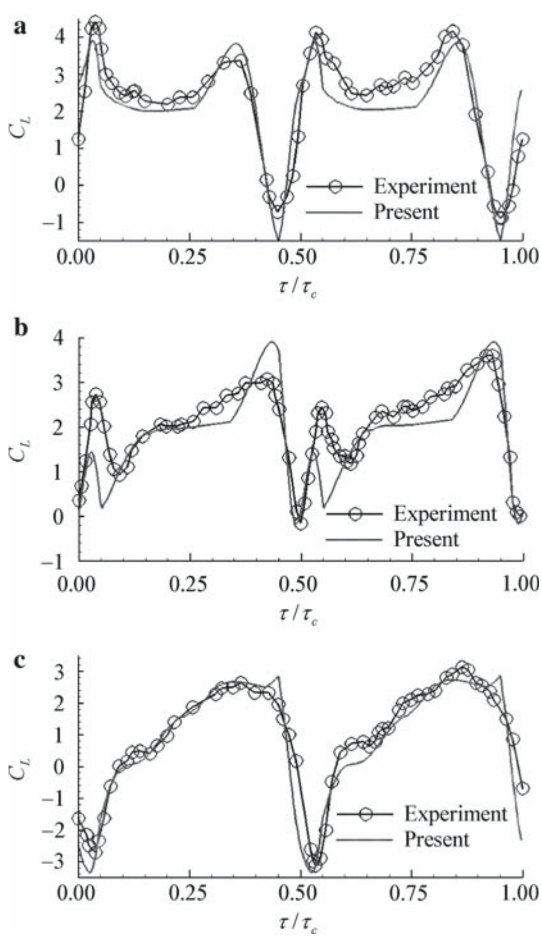

Fig. 5 Comparison of the results between the present CFD and Dickinson's [5] experiment. **a** Advanced mode; **b** symmetrical mode; **c** delayed mode

The comparison of the lift coefficients in the three modes between the present CFD and Dickinson's [5] experiments are illustrated in Fig. 5. Then the good agreement shows that the numerical method developed by Rogers and the computational program developed by author are suitable to the simulation of the flapping motion at Low Reynolds number.

5.2 Aerodynamic characteristics of the new bionic flapping motion

The study on the fruit fly hovering reveals four unsteady mechanisms to generate high lift. They are the delayed stall, the fast pitching-up rotation, the rapid acceleration and the rapid deceleration mechanisms. In this new bionic flapping motion, the delayed stall, the rapid acceleration and rapid deceleration mechanisms are kept, except that the pitching-up mechanism is replaced by pitching-down mechanism. Then, what are the aerodynamic characteristic differences between the fruit fly flapping motion and the new flapping motion? It is another question to answer.

The symmetrical planform of the flapping wing in the new flapping motion is obtained through averaging the leading and the trailing edges of the fruit fly flapping wing (see Fig. 2b). For the new bionic flapping motion, the rotational axis should be located at the 50% chord position from the leading edge. In order to compare the aerodynamic characteristics of the new flapping with those of the fruit fly, the fruit fly flapping motions of the three modes are numerically simulated again, with the new flapping wing planform at the new rotational axis (see Fig. 6). The present CFD unsteady aerodynamic coefficients C_L and C_D of the new bionic flapping motions of the three modes are shown in Fig. 7.

From Fig. 7, for the new bionic flapping motion, the delayed stall mechanism is also the most important and dominant factor to obtain high unsteady lift. On the other hand, comparing with Fig. 6, the high lift peak at the end of stroke generated by pitching-up disappears, because the pitching-up is replaced by the pitching-down, while the high unsteady drag peaks at the beginning and the end of stroke decrease very much. The new bionic flapping motion maintains the high unsteady lift mechanism and gets rid of the high unsteady drag mechanism very much. The ratio of lift to drag increase greatly.

In the symmetrical mode, a high lift peak and a small drag peak occur at the beginning of a stroke, both the lift and drag coefficients drop at the end of a stroke. From Figs. 4 and 7, it is shown that at the beginning of a stroke, the peaks of the lift and drag coefficients correspond to the rapid acceleration. Meanwhile the angle of attack increases from 0° to 40°. These peaks are also generated by the pitching-up with the acute angle of attack. At the end of a stroke, the coefficient drop corresponds to the rapid deceleration, with the angle of attack decreasing from 40° to 0°. In the middle of a stroke, the

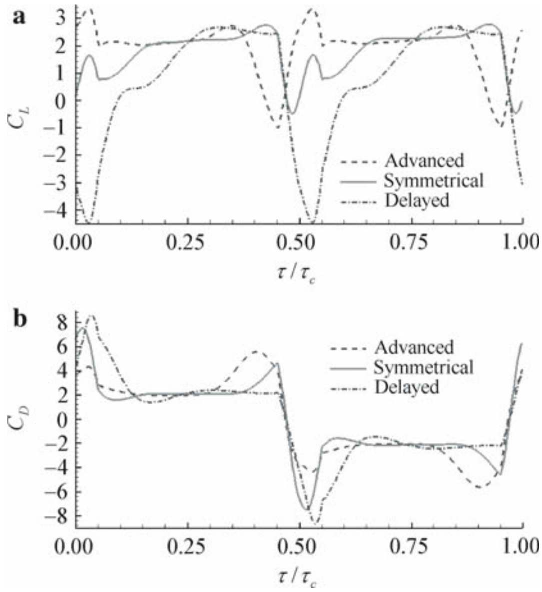

Fig. 6 Computational results of the three flapping modes of the fruit fly flapping motion with new flapping model wing and rotational axis located at 50% chord position. **a** Unsteady lift coefficient; **b** unsteady drag coefficient

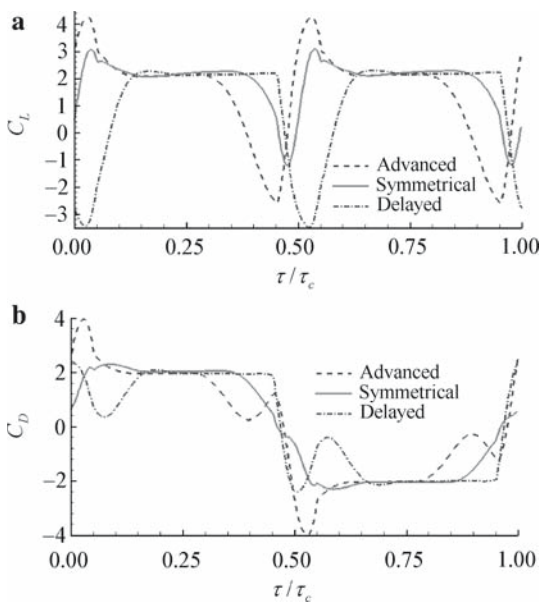

Fig. 7 Computational results of the new bionics flapping motion in three modes with new flapping model wing and rotational axis located at 50% chord position. **a** Unsteady lift coefficient; **b** unsteady drag coefficient

delayed stall mechanism generates the high unsteady lift and drag, which is also the most important mechanism to generate the lift.

Compared with the symmetrical mode, the advanced mode maintains the aerodynamic coefficient plateau generated by the delayed stall mechanism in the middle of a stroke. Since the pitching-down rotation precedes the stroke reversal by 8%, the aerodynamic force plateau of the advanced mode ends and drops earlier than that of the symmetrical mode. At the end of a stroke a larger negative lift coefficient peak appears, and the drag coefficient begins to decrease with fluctuation. When the flapping wing pitching-down rotates at the constant translational velocity, the angle of attack decreases from 40° to 0°. This makes both the lift and drag coefficients decrease. Subsequently, when the angle of attack goes on decreasing from 0° to −15°, the lift continues to drop while the drag increases. As the angle of attack changes from −15° to −29°, the translation begins to decelerate. Cooperating with the negative angle of attack, the added mass effect of the air around the wing makes the pressure at the lower surface of the wing increase and the pressure at the upper surface decrease, thus the lift suddenly increases. At the same time, the inertial force of the air around the wing pushes the wing in the moving direction. Then the drag decreases rapidly, when $\tau/\tau_c = 0.474{-}0.500$, it turns to thrust. After that, the next stroke begins accelerating. The angle of attack turns into positive and increases from 29° to 40°. Because the initial angle of attack in the advanced mode is greater than that in the symmetrical mode, the lift and drag coefficients are much greater than those in the symmetrical mode.

In the delayed mode, the most important and dominant factor for generating high aerodynamic coefficient is still the delayed stall mechanism. Different from the advanced mode, the angle of attack is negative acute in the delayed mode at the beginning of the acceleration. Thus a high negative lift peak and a high drag peak are generated. While the negative acute angle of attack changes rapidly to 0°, the negative lift coefficient peak and drag coefficient peak drop rapidly. Since the initial angle of attack is small and the time for rotational acceleration is relatively long, the lift and drag peaks in the delayed mode are very small.

5.3 Comparison between the new bionics flapping and the fruit fly flapping

The unsteady coefficients of the three modes of the fruit fly flapping motion were illustrated in Fig. 6. The model wing was the same as the one shown in Fig. 2c. From Fig. 6, it can be easily seen that: (1) The drag coefficient is often greater than the corresponding lift coefficient. At the beginning of a stroke, the drag coefficient is even two times of the lift coefficient; (2) The phase difference between the rotation and the translation has a significant influence on the lift coefficient. The average drag coefficient changes slightly. The average lift and drag coefficients and the ratio of lift to drag of the fruit fly flapping and those of the new bionics flapping are listed in Table 1. The drag coefficients are calculated by averaging the absolute values.

From Figs. 6, 7, and Table 1, we have the following findings in the new bionic flapping motion:

For the lift coefficient: (1) The delayed stall mechanism is preserved. Especially in the delayed mode, the lift coefficient plateau is much smoother than that of the fruit fly flapping; (2) The second aerodynamic lift peak at the end of a stroke disappears because the pitching up is replaced by the pitching down. In summary, compared to the general fruit fly flapping, the changes of the average lift coefficient in the new flapping manner decreases by 20.8% in the advanced mode, increases by 5.3% in the symmetrical mode, and increases by 45.3% in the delayed mode. The lift coefficient in the delay mode increases significantly. The great discrepancies of the average lift coefficients among the different flapping modes are greatly smoothed.

For the drag coefficient: (1) The drag coefficient peak deceases significantly. The maximum value of the drag coefficient is less than half of that of the fruit fly flapping motion; (2) The second drag coefficient peak disappears; (3) The drag coefficient plateau is shortened greatly in both the advanced mode and the delayed mode. The low drag coefficient zone appears at the rearward in the advanced mode and at the frontward in the delayed mode. The average drag coefficient of the new flapping is 41.4% smaller than that of the fruit fly flapping in the advanced mode, 36.6% smaller in the symmetrical mode and 41.9% smaller in the delayed mode.

The reason for these differences lies in the fact that the pitching-up rotation in the fruit fly flapping motion is replaced by the pitching-down rotation in the new bionic flapping motion. The most important advantage taken by the new bionic flapping is the substantial increase of the ratio of lift to drag through greatly reducing the average drag coefficient. The ratio of the lift to drag increases 35.0% in the advanced mode, 66.1% in the symmetrical mode and 150.0% in the delayed mode. These mean that for the new flapping motion less energy is needed to overcome the drag, so that the mechanism efficiency is enhanced.

6 Conclusions

At first, the numerical method used in this paper was verified by comparing the present CFD results with Dickinson's experimental results. Then by analyzing the regular and aerodynamic characteristics of the fruit fly flapping motion, the disadvantages of the fruit fly flapping motion were pointed out, and a new bionic flapping motion was proposed in this paper. The aerodynamic characteristics of the new bionic flapping motion were studied and compared with those of the fruit fly flapping motion in details. For the fruit fly flapping motion, the delayed stall mechanism and the rapid acceleration and rapid deceleration mechanisms at the end of a stroke generate the high unsteady lift. These mechanisms are fully utilized by the new bionic flapping motion. On the other hand, although the pitching-up rotation mechanism at the end of a stroke generates the high lift peak, it also generates the high drag peak, which is approximately two times of the lift peak. Then, in order to get rid of the disadvantage of this mechanism in the new bionic flapping motion, the pitching-up rotation is replaced by the pitching-down rotation at the end of a stroke.

For the new flapping motion, although the high lift peak generated by the pitching-up rotation disappears, the high drag coefficient peak decreases greatly. Thus compared with the fruit fly flapping motion, the ratio of the mean lift to the mean drag of the new flapping motion substantially is 35.0% greater in the advanced mode, 66.1% greater in the symmetrical mode and 150.0% greater in the delayed mode. Therefore the consumption of the energy to overcome the flapping drag greatly decreases and the energy efficiency increases very much. Meanwhile, compared with the fruit fly flapping, the aerodynamic characteristics of the delayed mode of the new bionics flapping significantly improve. The great aerodynamic discrepancies among the three different modes in the fruit fly flapping are effectively smoothed in the new bionic flapping.

Finally, it must be pointed out that the above conclusions are just drawn for the hovering flapping motion. And the aerodynamic characteristics of the new bionic flapping motion in forward flight are going to be studied in the next step.

References

1. Robert Burton: Bird Flight, Facts on File, New York (1990)
2. Theodorsen T.: General theory of aerodynamic instability and the mechanism of flutter. NACA report 496 (1935)
3. Osborne, M.F.M.: Aerodynamics of flapping flight with application to insects. J. Exp. Biol. **28**, 221–245 (1950)
4. Dickinson, M.H., Gotz, K.G.: Unsteady aerodynamic performance of model wings at low Reynolds numbers. J. Exp. Biol. **174**, 45–64 (1993)
5. Dickinson, M.H, Lehmann, F.O., Sane, S.P.: Wing rotation and the aerodynamic basis of insect flight. Science **284**, 1954–1960 (1999)
6. Ellington, C.P., Van den Berg, C., Willmott, A.P., Thomas, A.L.R.: Leading-edge vortices in insect flight. Nature **384**, 626–630 (1996)
7. Sun, M., Tang, J.: Unsteady aerodynamic force generation by a model fruit fly wing in flapping motion. J. Exp. Biol. **205**, 55–70 (2002)
8. RamamurtiR. Sandberg, W.C.: A three-dimensional computational study of the aerodynamic mechanisms of insect flight. J. Exp. Biol. **205**, 1507–1518 (2002)
9. Sun, M., Du, G.: Lift and power requirements of hovering insect flight. Acta Mech. Sin. **19**(5), 458–469 (2003)
10. Wu, J.H., Sun, M.: The influence of the wake of a flapping wing on the production of aerodynamic forces. Acta Mech. Sin. **21**(5), 411–418 (2005)
11. Sun, M., Wang, J.K., Xiong, Y.: Dynamic flight stability of hovering insects. Acta Mech. Sin. **23**(3), 231–246 (2007)
12. Yu, Y.L, Tong, B.G., Ma, H.Y.: An analytic approach to theoretical modeling of highly unsteady viscous flow excited by wing flapping in small insects. Acta Mech. Sin. **19**(6), 508–516 (2003)

13. Yu, Y.L., Tong, B.G.: A flow control mechanism in wing flapping with stroke asymmetry during insect forward flight. Acta Mech. Sin. **21**(3), 218–227 (2005)
14. Rogers, S.E., Kwak, D.: An upwind differencing scheme for the incompressible Navier–Stokes equations. Appl. Numer. Math. **8**(1), 43–64 (1991)
15. Weis-Fogh, T.: Quick estimates of flight fitness in hovering animals, including novel mechanism for lift production. J. Exp. Biol. **59**, 169–230 (1973)
16. Vogel, S.: Flight in drosophila. II. Variations in stroke parameters and wing contour. J. Exp. Biol. **46**, 383–392 (1967)